RSC Advances

ROYAL SOCIETY OF CHEMISTRY

www.rsc.org/advances

Hydrophilic modification of ordered mesoporous carbon supported Fe nanoparticles with enhanced adsorption and heterogeneous Fenton-like oxidation performance

Chunming Zheng[a,*], Xiangzhi Cheng[a], Chuanwu Yang[a], Caojin Zhang[a], Huilin Li[a], Lixin Kan[a], Jun Xia[a], Xiaohong Sun[b,*]

[a] *State Key Laboratory of Hollow-fiber Membrane Materials and Membrane Processes, School of Environmental and Chemical Engineering, Tianjin Polytechnic University, Tianjin 300387, P.R. China*

[b] *Key Laboratory of Advanced Ceramics and Machining Technology, Ministry of Education, School of Materials Science and Engineering, Tianjin University, Tianjin 300072, P.R. China*

* Corresponding author. Tel.: +86 022 83955661; fax: +86 022 83955140.

E-mail address: zhengchunming@tjpu.edu.cn (C.M. Zheng).

* Corresponding author. Tel.: +86 022 27406141; fax: +86 022 27406114.

E-mail address: sunxh@tju.edu.cn (X.H. Sun).

Abstract

In this study, ordered mesoporous carbon catalyst containing uniform iron oxide nanoparticles (Fe/meso-C) has been synthesized and surface hydrophilic modified with hydrogen peroxide, which shows excellent adsorption and heterogeneous Fenton degradation performance for methylene blue (MB). With the characterization such as XRD, TEM, SEM, TG and N_2 sorption-desorption isotherms, Fe/meso-C treated with hydrogen peroxide (H-Fe/meso-C) maintained hexagonally arranged mesostructure, uniform mesopore size (~2.3 nm), high surface area (up to 530 m^2/g) and moderate pore volume (0.29 cm^3/g) as untreated catalyst. The Fe_2O_3 nanoparticles highly dispersed in the carbon framework and mesopore channels. The hydrophilicity of the catalysts surface also improved after the H_2O_2 modification. As a milder oxidizing agent, hydrogen peroxide is used to introduce the oxygen-containing group on the carbon surface. Due to the hydrophilic surface and retaining mesoporous structure, H-Fe/meso-C catalyst presents a better Fenton-like catalytic performance than Fe/meso-C. The adsorption and heterogeneous Fenton-like degradation of MB achieved 96 % in 220 min with the optimal oxidation conditions of 30 mg/L MB solution, 0.7 g/L catalyst, 50 mmol/L H_2O_2 and initial pH.

Key words: Fe nanoparticles; ordered mesoporous carbon; surface hydrophilic modification; heterogeneous Fenton

1. Introduction

Nowadays, protection and preservation the quality of the water resources is one of the most critical tasks to maintain the quality of our lives and ensure the sustainable development in many regions around the world.[1,2] The nature of the refractory pollutants present in water is quite variable. Particular attention should be made to the pollution of water by synthetic dyes in the textile industry.[3] Actually, the removal of synthetic dyes from wastewater is really challenging to the related industries, since the synthetic dyes used are stable compounds, difficult to destroy by common wastewater treatments. Among the different approaches for the dyes elimination, advanced oxidation processes (AOPs) are becoming important technologies for the dye wastewater treatment.[4] And the Fenton reaction is the most intensively investigated AOPs. Compared to the homogeneous Fenton, heterogeneous Fenton attracted more attention for the wider working pH and less iron sludge generation.[5,6]

In heterogeneous Fenton reactions, Fe-based catalysts have recently attracted ever growing concern because of their combined simplicity, efficiency and low investment cost for reusability.[3] Different iron oxides and iron hydroxides as heterogeneous Fenton-like catalysts have been studied, such as hematite, goethite and magnetite.[7] However, many of these catalytic systems do not exhibit favorable degradation activities, which is especially due to that Fe^{3+} cannot effectively catalyze the generation of ·OH from H_2O_2. In this regards, the impregnation method has been used to deposit iron species onto different types of solid supports (e.g., clays, zeolites and carbon materials).[1,8] In all of these supports, carbon materials has been intensively

investigated due to its combination of low price, high porosity and surface area, stability in acidic and basic media, and easily tunable surface chemistry, which could be difficult to be replaced by other kinds of inorganic supports and efficiently enhance the performance of heterogeneous Fenton reactions.[9] Furthermore, carbon materials could also adsorb the pollutant or even be catalysts by themselves, once the surface of carbon materials have unpaired π electrons which can react with H_2O_2 leading to the generation of hydroxyl radicals.[4,10] Castro et al. prepared activated carbon supported iron oxide, which showed intense removal of the methylene blue through combined adsorption and oxidation processes.[11] Wang et al. synthesized high surface area mesoporous copper ferrite (meso-$CuFe_2O_4$) and discussed the superiority of bimetal catalyst since the redox properties of dissolved transition metal cations (Fe^{2+}, Cu^{2+}) allow generating highly active hydroxyl radicals in the presence of hydrogen peroxide.[12] Duarte et al. investigated the influence of the carbon particle size as Fe supports for removal of the azo dye Orange II.[13] With the decrease in carbon particle size, the dispersion of iron in the catalysts was improved, which also favored the catalytic activity. Then they studied the textural and chemical surface properties of fresh and spent activated carbon during the heterogeneous Fenton processes. And the dye removal efficiencies of these catalysts were varied with the different interactions of the oxidized products with the carbon supports.[14] Karumuri's research showed that the hydrophilic properties of carbon supports could have significant influence in catalytic oxidation.[15] To the best of our knowledge, the surface properties of carbon based heterogeneous Fenton catalysts, especially the hydrophilic nature of carbon

supports, have not thoroughly investigated. The carbon supported catalysts still face the obvious problems like instability in reuse, low amount of iron loading and inconvenience in recycling.[16,17]

As a new kind of carbon nanomaterials, ordered mesoporous carbons have been proved to be excellent catalytic supports due to their well-controlled pore structures, high surface areas, uniform and tunable pore sizes and good electrical conductivity and thermal stability.[18,19] Undoubtedly, ordered mesoporous carbons incorporated with iron nanoparticles could hold great promise in developing high performance iron-based heterogeneous Fenton catalysts. Ordered mesoporous carbons with incorporated functional nanoparticles can be synthesized through either a hard-templating approach or soft-templating approach.[20] For example, Kim et al. have synthesized magnetic ordered mesoporous carbon with impregnation method.[21] However, the Fe nanoparticles in the above-reported mesoporous carbon suffer severe aggregation with broad size distributions. Additionally, a variety of mesoporous carbons embedded with metal oxides nanoparticles have reported by the use of previously synthesized inorganic nanoparticles as a metallic precursor. The synthesis processes could be less controllable for the capped nanoparticles cannot be well dispersed in the solution of carbon precursors and templates.[8,22,23] Recently, Zhao and his co-workers fabricated ordered mesoporous carbon with acetylacetone chelated-assisted co-assembly to iron nanoparticles.[24] The iron-containing nanoparticles are partially embedded with the remaining part exposed in the mesopore channels. Nevertheless, this multi-step approach is rather low efficiency and high cost.

Meanwhile, the surface of carbon support was not hydrophilic modified for the carbon support was made from phenolic resin. The degradation performances of all these kinds of catalysts were limited since the heterogeneous Fenton reaction was carried out in aqueous conditions. So, some special functional groups are introduced in the carbon matrix surface to increase the hydrophilic and acid properties, such as hydroxyl, phenol, lactone and other groups with oxidation treatment. In order to retain the mesoporous structure of such catalyst, mild oxidation agents, such as hydrogen peroxide, should be used to the modification processes.[25]

Herein, we demonstrate surface hydrophilic modification route for the synthesis of high-quality ordered mesoporous carbons incorporated with highly dispersed uniform Fe nanoparticles as heterogeneous Fenton-like oxidation catalyst, which shows enhanced adsorption and degradation performance of methylene blue (MB). The synthesis is accomplished by slow evaporation of ethanol solution with resol and ferric nitrate as the precursors and triblock copolymer F127 as a template. Then the catalysts were hydrophilic modified by hydrogen peroxide with different concentrations. During the heterogeneous Fenton reaction of MB, hydrogen peroxide modified Fe-based mesoporous carbon catalyst shows higher activity and stability than untreated catalyst in the adsorption and degradation processes, which is due to the unique nanostructure and high porosity of the catalysts. The effects of further H_2O_2 oxidation treatment of the nanocomposites on removal of dye molecule were studied in detail.

2. Experimental

2.1. Materials

Poly(ethylene oxide)-*block*-poly(propylene oxide)-*block*-poly(ethylene oxide) triblock copolymer Pluronic F127 (Mw =12600, $PEO_{106}PPO_{70}PEO_{106}$) purchased from Sigma Aldrich was used as templates, phenol, formalin solution (37 *wt*%), sodium hydroxide, hydrochloric acid, ethanol, acetylacetone received from Tianjin Chemical Corp. and ferric nitratenonahydrate ($Fe(NO_3)_3 \cdot 9H_2O$) were used as the salt precursor. Methylene blue, sodium hydroxide (NaOH), H_2O_2 (30 wt%) and other chemicals used in this study were analytical grade and used without further purification.

2.2. Synthesis and modification of H-Fe/meso-C catalysts

The mesoporous carbon materials were synthesized following the procedure reported by Zhao and Wang et al.[26] The mesoporous Fe/meso-C composites were synthesized using the multicomponent co-assemble method with Pluronic F127 as the template in an ethanol solution. In the typical synthesis, 5.0 g phenol was melted at 40- 42 °C, then 1.06 g NaOH (20 *wt*%) aqueous solution was added under stirring for 10 min. Then 8.8 g formalin solution (37 *wt*% formaldehyde) was added slowly and heated at 70 °C for 60 min. After cooling to room temperature, the pH value of the solution was adjusted to about 6.0 with 2.0 mol/L HCl solution. The resol precursors were re-dissolved in ethanol (20 *wt*%) and sodium chloride was separated as a precipitate. The Fe/meso-C was obtained using ferric nitrate following the chosen

weight ratio of F127: resol: Fe_2O_3: ethanol=1:1:0.04:17. 0.2 g $Fe(NO_3)_3 \cdot 9H_2O$ was added into 5.0 g resol precursor solution. After further stirring at 50 ℃ for 30min with a condenser tube, the mixture was transferred into petri dishes, followed by evaporation of ethanol for 8 h at room temperature and 100 ℃ for 24 h. The obtained composite films were scrapped off and calcined at 600 ℃ in N_2 for 3 h. The temperature rate was 1 ℃/min. The carbonized samples were denoted as Fe/meso-C.

The ordered mesoporous carbon co-assembled with Fe nanoparticles was further treated by H_2O_2 to enhance their hydrophilic properties. In detail, 0.5 g Fe/meso-C was added into 8 g of 5~ 15 wt% H_2O_2 solution at room temperature, then the reaction mixture was stirred at 60 ℃ for 30 min. After separation with a magnet and washing with ethanol, the magnetic nanocomposites were dried at 100 ℃ for 4 h. The resulting catalysts were grounded thoroughly and denoted as H-Fe/meso-C. Fig. 1 illustrates the fabrication and H_2O_2modification processes of ordered mesoporous carbon supported Fe nanoparticles.

2.3. Characterization

The crystalline phasesin the materials were studied by X-ray diffraction techniques on Philips X'pert instrument with Cu Kα radiation source in the 2θ range of 0.5-10˚. Metal dispersion on the carbon surface and the nature of the particles were analyzed by HRTEM and SEM using Hitachi H-7650 transmission electron microscope and Hitachi S-4800 scanning electron microscope. Nitrogen sorption-desorption isotherms were measured at 77 K with Micromeritics Tristar

3000 analyzer after outgassed at 423 K for a minimum 12 h. The Brunauer−Emmett−Teller (BET) method was utilized to calculate the specific surface areas (S_{BET}) in a relative pressurerange from 0.05 to 0.25. The Barrett−Joyner−Halenda (BJH) model was used to study the pore volumes and size distributions, and the total pore volumes (V_t) were estimated at a relative pressure P/P_0 of 0.995. X-ray photoelectron spectroscopy was measured on a Kratos ASIS-HS X-ray photoelectron spectroscope equipped with a standard and monochromatic source (AlKα) operated at 150 W (15 kV, 10 mA). Thermogravimetricanalysis (TGA) curves were carried out using a TA SDT-Q600 analyzer from 25 to 900 °C at a heating rate of 5 °C/min in airflow of 80 mL/min. FT-IR was taken with a Bruker TENSOR37 FT-IR spectrometer transmission analyzer in KBr pressed pellets. The concentration of MB in the supernatant liquid was determined at the absorbance peak of 664 nm with UV-vis spectrophotometer (UV-752, Shanghai Rex Instrument Co., Ltd., China). ·OH concentration was determined by the benzoic acid ($C_7H_6O_2$) fluorescence method.[27] The photoluminescence spectra (PL) of benzoic acidsamples were obtained by using a Fluorescence Spectrophotometer (F-380, Tianjin GangdongInstrument Co., Ltd., China.) at the excitation wavelength of 325 nm.

2.4. Catalytic tests

The catalytic experiments were carried out in a batch reactor at ambient atmosphere and 30 °C. All the experiments were carried out in a stirred slurry batch reactor with

the temperature controlled by a thermostatic bath. In a typical experiment, certain amounts of catalysts were dispersed in 50 mL MB solution (30 mg/L). After stabilization of temperature and pH (adjusted with 0.1 mol/L HCl solution), the suspensions were magnetically stirred for about 30 min to achieve adsorption/desorption equilibrium between the dye and catalyst. Then, a certain amount of H_2O_2 was added to the above suspensions. At given intervals of degradation, 2 mL reaction solution was sampled and immediately centrifuged to remove the catalyst for analysis. Mineralization was evaluated by TOC analyses in a Shimadzu TOC-VWP equipment and iron leaching was quantified in an Varian Vista inductively coupled plasma atomic emission spectroscopy (ICP-AES, America) with the wavelength range of 167-785 nm and the limit detection of 0.01 μg/L.

3. Results and discussion

3.1. Characterization of as-prepared carbon-basedcatalysts

Small-angle and wide-angle X-ray diffraction (SAXRD and WAXRD) patterns are illustrated in Fig. 2. As is shown in Fig. 2A, the samples of mesoporous carbon and Fe/meso-C show a wide peak at about 0.70°, which related to the reflections a of 2-D hexagonal meso-structure carbon. However, compared with above catalysts, the H-Fe/meso-C presents a broader diffraction peak, which indicates that the mesoporous structures are slightly deteriorated but not destroyed with the modification of hydrogen peroxide. In the wide-angle XRD patterns as shown in Fig. 2B, five resolved diffraction peaks (30.1°, 35.5°, 43.1°, 57.3°, 62.7°) were observed in

the Fe/meso-C, which can be assigned to 220, 311, 400, 511 and 440 reflections of crystalline γ-Fe_2O_3 phases (JCPDS Card No.89-5892). These results indicate that the iron-oxide nanoparticles are well crystallized and uniformly dispersed in the carbon matrix.[26] The H-Fe/meso-C catalysts reveal the similar diffraction patterns as the Fe/meso-C sample, suggesting that the hydrogen peroxide treatment has no significant influences on the well-crystallized mesoporous structure of these catalysts. To further investigate the crystal nature and influence of temperature on the type of iron-based particles, H-Fe/meso-C catalyst was calcined at 800 °C for 3 h under N_2 atmosphere. The WAXRD patterns are shown in Fig. 3. In Fig. 3, the catalysts show the same six resolved diffraction peaks of crystalline γ-Fe_2O_3. And another five diffraction peaks also emerged in the calcined H-Fe/meso-C patterns. Among them, the diffraction peaks at 31.4°, 39.7° and 49.7° maybe attributes to α-Fe_2O_3, 43.0° contributes to Fe_3C and 45.2° contributes to iron nanoparticles formed by in situ reduction during the calcination.

To further investigate the porous structure and the distribution state of iron species of Fe/meso-C and H-Fe/meso-C catalysts, SEM (EDS elemental mapping characterization included) and TEM characterizations were carried out and related images of above catalysts are shown in Fig. 4 and Table 1. There were more than ten images for each sample in the characterizations of SEM and TEM imaging. Although several taken images with great differences exist, which taken for the catalysts samples, most of the pictures still remain similar for the morphologies of these catalysts. By comparing the SEM images of Fe/meso-C (Fig. 4A) and H-Fe/meso-C

(Fig. 4B) catalysts, the characterization of the surfaces roughness of these catalysts is obtained from the brightness differences between separation distances of these catalysts. Evidence shows that an increased roughness of catalyst surface after hydrogen peroxide treatment could be observed for a correlation between the texture and the fractal dimension of the feature images. After the 5 wt% hydrogen peroxide treatment of Fe/meso-C, the particle size of the catalyst also remains little change. The elemental distribution mapping results of above catalysts given by EDS characterizations were shown in Fig. 4C and D. The EDS elemental maps confirm that Fe element is highly dispersed in Fe/meso-C and H-Fe/meso-C.[28] Hydrogen peroxide treatment did not change the uniform distribution of Fe in the carbon based catalysts. From relative atomic content of existing elements shown in Table 1, the oxygen content on the mesoporous carbon supports greatly improved after the hydrogen peroxide treatment with the H-Fe/meso-C, indicating the increase of surface oxygen-containing groups caused by the oxidation of the hydrogen peroxide. The H-Fe/meso-C surface behaved more hydrophilic for the increased numbers of oxygen-containing groups.[15] The uniform distribution of Fe element on the catalysts surface was also confirmed by the TEM characterization. The TEM images of Fe/meso-C (Fig. 4E) and H-Fe/meso-C (Fig. 4F) show stripe-like and hexagonally arranged pore morphology.[29] The as-made H-Fe/meso-C possesses highly uniform mesostructure with 2-D hexagonal pore symmetry and a mean pore size of about 5.4 nm, just as indicated in Fig. 4F. In the Fig. 4E and F, the Fe/meso-C preserves the long ordered arrangement of the lattice fringes and the iron oxide nanoparticles are

well incorporated in the carbon framework, which are in accordance with the XRD measurements. The size distribution curves of Fe_2O_3 nanoparticles displays a mean diameter centered at ~12 nm with a standard deviation of about 5 % of 100 nanoparticles by Nano Measurer (Fig. 4E). After 5 wt% hydrogen peroxide treatment for Fe/meso-C, Fe_2O_3 nanoparticles of ~20 nm can be obtained without aggregation (Fig. 4F). Meanwhile, the porous structure of H-Fe/meso-C which originates from the structure of Fe/meso-C still remained.

The thermo-gravimetric analysis (TGA) was commonly performed under air flow to estimate the thermal stability and phase purity of Fe_2O_3 nanoparticles incorporated mesoporous carbon. The detailed results after charring the catalysts are shown in Fig. 5. The weight change of the bulk Fe_2O_3 might come from some organic impurities. There exists a slight weight loss of Fe/meso-C and H-Fe/meso-C below 150 °C, which is attributed to the adsorbed water. The sharp weight loss in the temperature range of 400-600 °C was owing to the burn of carbon. The synthesized Fe/meso-C exhibits the narrow temperature range, indicating the highly analogous pore structure of the catalysts. The sharp weight loss of the H-Fe/meso-C happens at lower temperature and the depressing process has a wider range than pure Fe/meso-C, which also confirmed the numbers of organic groups on the catalyst surface increased after the hydrogen peroxide treatment.[30,31] By the TG characterization of these catalysts, the weight percentage of the residues is about 6.2 %, corresponding to the received Fe_2O_3 from the oxidation of iron oxides in the Fe/meso-C catalysts.

N_2 adsorption-desorption isotherms (Fig.6) of these carbon-based catalysts show

typical type-IV curves, which reflects a high uniformity of mesopore size and the similar pore structures.[32,33] The BET surface areas of the mesoporous Fe/meso-C and H-Fe/meso-C are 532, 561 m^2/g and the pore volumes have no obvious change. When iron doped into ordered mesoporous carbon, the BET surface area and mean pore size of Fe/meso-C increased, which confirms that metal doping of the carbon support may increase BET surface area and pore size of mesoporous carbon. The reason might be the shrinkage of carbon matrix could be hindered by the iron entrapped into the support during the carbonization process.[22] After the hydrogen peroxide treatment, the BET surface area and pore size distribution of H-Fe/meso-C further increased, indicating the etching of carbon surface with H_2O_2. Some new mesopores can be generated or the adjacent mesopores become united during the etching processes.[24]

XPS characterization was also used to analyze the chemical environment and oxidation state of the carbon-based catalysts. As shown in Fig. 7A, Fe/meso-C exhibited wider peak of O_{1s} element than meso-C samples, which attributed to the generated γ-Fe_2O_3, C-O or other phases in the Fe/meso-C during the carbonization processes.[34] After the hydrogen peroxide treatment, H-Fe/meso-C showed abnormity O_{1s} peak for the introducing of oxygen-containing groups on the catalyst surface. In Fig. 7B, the spectrum peaks of $Fe2p_{3/2}$ and $Fe2p_{1/2}$ in Fe/meso-C were about 711.0 eV and 724.8 eV, respectively.[35] After the hydrogen peroxide modification, the spectrum peaks of $Fe2p_{3/2}$ and $Fe2p_{1/2}$ in H-Fe/meso-C changed to 710.5 eV and 724.1 eV, which might be due to the bond generated by iron and oxygen-containing group.[36]

In the FT-IR spectrum of the carbon-based mesoporous catalysts (Fig. 8), the

band at 3425 cm^{-1} arising from vibrational stretching of the -OH groups was stronger and broader after the hydrogen peroxide treatment. It indicates that more -OH functional groups might be generated in the carbon framework. The two bands at 1612 and 1200 cm^{-1} assigned to the C-C and C-O stretching vibration broadened, which also confirmed above results.[37,38] With the hydrogen peroxide treatment, H_2O_2 oxidized the active sites such as $-CH_2$ and -CH groups of the carbon framework into -C-OH and -C=O groups with the elimination of CO_2 species. It derives from the etching of the carbon walls, and the BET surface area and mean pore size sequentially increased from this etching effect.[24]

The hydrophilic test results of the mesoporous carbon-based catalysts were listed in Table 2, the Fe/meso-C showed a surface hydrophobic property due to its static water contact angle of 113.49°. After the modification with hydrogen peroxide, the H-Fe/meso-C catalyst contact angle decreased, which suggested the surface hydrophilic nature was enhanced.[15] With the increase of H_2O_2 concentration, H-Fe/meso-C surface became more hydrophilic, which was due to the increased oxygen-containing groups numbers during the hydrogen peroxide treatment of the catalysts.

3.2. Comparison and efficient elimination of MB with Fe/meso-C and H-Fe/meso-C

Since the co-existence of complex adsorption and oxidation during the heterogeneous Fenton processes, the adsorption processes of MB were firstly studied with Fe/meso-C and H-Fe/meso-C. A batch reactor with 50 mL was employed to carry

out the adsorption kinetic study of MB. According to the result, 50 mg carbon-based catalysts were added into a certain concentration of MB solution with continuously magnetic stirring with pH adjustment. Prior to the adding of H_2O_2, the adsorption processes of MB could be investigated on all samples in the first 30 min, then the certain amount of hydrogen peroxide was added (Fig. 9). The heterogeneous Fenton-like oxidation began and the elimination efficiencies of MB were measured at certain interval.[30] All these degradation experiments have been carried out with triplicate samples.

The adsorption and degradation of several carbon-based catalysts used in the MB elimination processes were shown in Fig. 9. There was a little elimination in the procedures of meso-C and α-Fe_2O_3, which indicated that the saturated extent of adsorption of Fe/meso-C was limited and the mesoporous structure of the catalysts offered great advantages in the heterogeneous Fenton-like oxidation reaction. With the modification of introducing the oxygen-containing groups, the H-Fe/meso-C catalyst exhibited a higher constant of degradation rate than meso-C and α-Fe_2O_3 (Fig. 9B), which was the result that the catalyst after hydrogen peroxide treatment was more hydrophilic and could completely dispersed in the solution. However, the differences of degradation rates between H-Fe/meso-C and unmodified Fe/meso-C catalyst are not very significant, especially the first used cycle of H-Fe/meso-C and unmodified Fe/meso-C. The data of batch reuse performances for H-Fe/meso-C and unmodified Fe/meso-C also shown in Fig. 12A and B. The degradation rate constants for H-Fe/meso-C (0.562 h^{-1}) are even lower than that of Fe/meso-C (0.617 h^{-1}).

Especially, the first hour of the degradation rate for H-Fe/meso-C is even much slower than that of Fe/meso-C. In the second and third run of these catalysts, the degradation rates of H-Fe/meso-C obviously increased (0.608 h^{-1} and 0.397 h^{-1}), and they are obviously higher than those of Fe/meso-C (0.271 h^{-1} and 0.112 h^{-1}). In order to clarify this problem, H-Fe/meso-C was treated with distilled water (none of hydrogen peroxide added) again, which was labeled as W-Fe/meso-C. After the degradation tests of MB for W-Fe/meso-C, the degradation rate of W-Fe/meso-C (0.953 h^{-1}) was much higher than that of H-Fe/meso-C and Fe/meso-C (0.562 h^{-1} and 0.617 h^{-1}). This might be due to the iron species adsorbed on Fe/meso-C also involved in the degradation processes, which similar results were also reported by Rodriguez et al.[39] For Fe/meso-C, the degradation rate increased since there are iron species adsorbed on the catalysts surface at the beginning of the processes. These iron species contributes to the degradation processes. With the leaving of these iron species from the Fe/meso-C catalysts surface, the degradation rates slightly decreased. Meanwhile, after H_2O_2 treatment and washing of H-Fe/meso-C, there is few iron species left on the H-Fe/meso-C catalysts surface. Therefore, the first hour of degradation rate of H-Fe/meso-C and W-Fe/meso-C were slower than that of Fe/meso-C. And the improvement of total degradation rates for H-Fe/meso-C and W-Fe/meso-C might be H_2O_2 and water washing treatments enlarged the mesoporous size during the processes. Therefore, more Fe_2O_3 nanoparticles embedded in the carbon framework exposed in the mesopore channel, which provided more active sites to participate in the Fenton-like catalytic reaction.[22] For the increased hydrophilic surface properties of

H-Fe/meso-C, the hydrogen peroxide could be more easily to access to the catalysts surface, hence the catalysts dosage could be reduced with the same degradation effect as the original Fe/meso-C.[38] In Fig. 12B and D, the degradation rate for repeated H-Fe/meso-C catalysts showed similar trends, which also confirmed above deduction. This made the difference of the increase of catalytic performance resulted from adsorbed iron species and porous change coming from H_2O_2 surface modification. Therefore, the treatment of H_2O_2 can improve the catalytic degradation by changing the porous and surface property. However, further research will be needed to clarify a detailed mechanism that explains the performance of this material as a heterogeneous Fenton-like catalyst.

The Fenton oxidation kinetics would be significantly affected by different initial parameters, such as pH, catalyst dosage, the concentration of H_2O_2 and so on. Therefore, various comparative experiments were carried out to investigate the experimental conditions of the Fenton-like oxidation reaction, as shown in Fig. 10. In Fig. 10A, the influence of catalysts dosage on the MB degradation performance was studied. With the increase of catalyst amount, the degradation rate of MB improved, which suggest that more catalyst supplies more active sites. Therefore, more active radicals could be achieved during the heterogeneous Fenton degradation processes. Meanwhile, adsorption of methylene blue also greatly increased with the catalyst dosage changing from 0.7 to 1.2 g/L. When the catalyst dosage increased, more mesoporous and microporous pores and channels in the catalysts could be obtained during the degradation processes, which could lead to the increased adsorption of

organic molecules. Meanwhile, the increased Fe species could react with ·OH to produce the hydroperoxyl radicals, which had little effect to the degradation.[40,41] Therefore, the excessive catalyst decreased the degradation rate of MB. The accumulation of the catalyst particles was thought to be another reason to this phenomenon.[42] Hence, the highly catalytic activity and elimination rate of MB could be gained in a certain limited catalyst dosage. And 0.7 g/L H-Fe/meso-C might be used in this Fenton-like oxidation system. The ultimate degradation rate could reach up to 96 %.

The initial pH value of the catalytic system also has the decisive influence on the elimination of the MB in the Fenton-like reaction system, which owes to the significant effect of the number of active species ·OH acting as the core role of this oxidation reaction. As shown in Fig. 10B, the study was conducted at the pH range from 4.0 to 8.0 in 0.7 g/L H-Fe/meso-C and 50 mmol H_2O_2. Among them, pH value of 7.33 was the original pH of the catalytic system without the adjustment with acid. From Fig. 10B, the appropriate pH to the degradation of MB was also at initial pH, which might be result from that in weak alkaline solutions, instead of O_2 and H_2O, more hydroxyl radical could be obtained in the decomposing of H_2O_2.[43] Therefore, following the H-Fe/meso-C Fenton-like reactions will be carried out at initial pH value.

Fig. 10C shows the influences of H_2O_2 concentration of carbon-based catalysts on MB degradation from 10 to 200 mmol/L. It could be clearly seen that the system containing 150 mmol/L H_2O_2 get the 96 % degradation at first, and then the

elimination of MB slightly decreased in the same period of time with 50 mmol/L H_2O_2. When H_2O_2 concentration was higher than 150 mmol/L, MB degradation slowed down and decreased. This is probably owing to the excessive H_2O_2 acts as the competitor to react with hydroxyl radicals (·OH) in advance and produces superoxide ($O_2^{\cdot-}$) and hydroperoxyl (HOO·) radicals that show less reaction rate than ·OH, which results to the low MB degradation.[36,44] Combined with the MB discoloration rate and economical utilize of the oxidant, 50 mmol/L was chosen to be the optimal H_2O_2 concentration.

3.3.Mineralization and the plausible degradation mechanism of H-Fe/meso-C

In order to investigate the plausible mechanism of the H-Fe/meso-C Fenton oxidation system, benzoic acid was used as a fluorescent probe to measure the generated ·OH radicals with a Fluorescence Spectrophotometer (F-380, Tianjin Gangdong Instrument Co., Ltd., China.) at the wavelength of excitation 325 nm.[27] In a typical experiment, the procedures were carried out under the conditions of 10 mmol benzoic acid, 50 mmol/L H_2O_2 and 1 g/L catalyst before and after the modification of hydrogen peroxide. In this experiment, benzoic acid could be easily reacted with ·OH radicals producing highly fluorescent *p*-hydroxybenzoic acid.

As can be seen in Fig. 11, H-Fe/meso-C Fenton-like oxidation system generated more ·OH radicals at the early period of experiment, which could cause a higher degradation rate in the heterogeneous Fenton processes of MB. After 30 minutes, the fluorescent intensity increased slowly both in the Fe/meso-C and H-Fe/meso-C

catalytic systems. Based on the results of XRD and determination of ·OH concentrations by fluorescence spectra, plausible mechanism of the heterogeneous Fenton-like reaction was proposed. According to the Haber-Weiss mechanism, the decomposition of H_2O_2 and degradation of MB mainly occurred on the iron oxide surface.[46] And Fe^{2+} also activates H_2O_2 to generate •OH on the catalyst surface.[23] Hence, the catalytic performance varied remarkably with the changes of surface properties of solid Fenton-like catalysts. For H-Fe/meso-C catalyst, the modification of H_2O_2 made the surface of catalyst more hydrophilic, which made it easy to expose more active sites contacting with H_2O_2 and the organic pollutant. Thus more Fe species attacked H_2O_2 molecules and more ·OH could be created to react with the organic dye during the degradation processes. Therefore, the H-Fe/meso-C exhibited a higher degradation rate in the Fenton-like catalytic oxidation system.[30]

3.4. Chemical reusability and stability of as-prepared carbon-based catalysts

The reusability and stability of the carbon-based catalysts were evaluated by repetitive reaction in three consecutive runs under identical conditions of 0.7 g/L catalyst, 50 mmol/L H_2O_2 and 30 mg/L MB solution. After each run, the catalyst was separated by filtration, washed with ethanol and deionized water, then dried at 100 ℃ for 6 h to carry out the next experiment. As shown in Fig. 12A and C, the kinetic analysis of the Fe/meso-C heterogeneous Fenton-like oxidation procedures shows that the degradation of MB follows the pseudo-first order. The apparent rate constants of Fe/meso-C for three different reuse batches are 0.617, 0.271 and 0.112 h^{-1} (Fig. 12C).

The initial catalytic activity of Fe/meso-C weakened gradually during the three cycles. This might be caused by the residual by-products and reactants adhered on the active sites of catalyst and small amount of iron leaching in the oxidation reaction and washing processes.[47] And it could also be further confirmed in the XRD and TEM patterns of Fe/meso-C observed in Fig. 2 and Fig. 4E, respectively.

As regard to the hydrophilic H-Fe/meso-C (Fig. 12B and D), the reusable heterogeneous Fenton-like reactions were carried out under the same conditions. Compared to the primary Fe/meso-C, the modified H-Fe/meso-C catalyst exhibited better stability of a higher degradation rate during the three reuse cycles. Among these processes, the catalytic activity slightly increased in the second run (0.562 h^{-1} versus 0.608 h^{-1}), which was quite different with the catalytic mechanism of ordered mesoporous composite components in heterogeneous Fenton-like processes, such as Fe-Cu and Fe-Zn composites.[48,49] The Fe-Cu and Fe-Zn composites influenced the catalytic activity by introducing the second metal, which increased the active sites and the synergetic effect of Cu or Zn to the Fe species on the surface of the catalyst, and then the components were more conducive to promote the interfacial electron transfer.[23] However, the degradation rate of H-Fe/meso-C changed by the modification of H_2O_2, which might be due to the more hydrophilic surface property and the enlarged mesoporous size. Therefore, more Fe_2O_3 nanoparticles embedded in the carbon framework could expose in the mesopore channel, which provides more active sites to participate in the Fenton-like catalytic reaction.[45] And the peroxide oxidation treatment also enhanced the reuse stability of H-Fe/meso-C catalyst. In this

study, the final degradation could reach to 96 % in 10 h and the leaching of iron could be neglected (0.73 mg/L) using inductively coupled plasma atomic emission spectroscopy (ICP-AES), which is much lower than the legal limit imposed by the directives of the European Union (2 mg/L).[50] Hence, H-Fe/meso-C catalyst has been proved to be an attractive alternative in the treatment of environmental refractory organic pollutants and have a unique and superb catalytic activity in the heterogeneous Fenton-like system.

4. Conclusions

In this study, ordered mesoporous carbon supported Fe_2O_3 nanoparticles has been surface hydrophilic modified with hydrogen peroxide, which shows enhanced adsorption and heterogeneous Fenton oxidation performance for methylene blue. The morphology, crystalline and structure of the catalysts before and after Fenton-like reaction were characterized with the XRD, TEM, TGA and N_2 sorption-desorption. The mesoporous structure of carbon support remains and the highly dispersed iron particles of the catalyst increase the degradation performance of MB after the hydrogen peroxide treatment. With the optimal oxidation conditions of 30 mg/L MB solution, 0.7 g/L catalyst, 50 mmol/L H_2O_2 and initial pH, the adsorption and heterogeneous degradation of MB could achieve about 96 % in 220 min. After the modification of hydrogen peroxide, the hydrophilic H-Fe/meso-C catalyst exhibits higher degradation rate in the Fenton-like catalytic system. Based on the small amount of iron leaching and the stability of the 2-D hexagonally arranged pore

structure, the ordered mesoporous carbon supported Fe nanoparticles treated by hydrogen peroxide could be used as a promising cyclically heterogeneous Fenton-like catalyst.

Acknowledgments

This work was supported by the National Natural Science Foundation of China (21101113, 51172157, 51202159, 51208357, 51472179, 51572192), Doctoral Program of Higher Education, Ministry of Education (20120032120017), General Program of Municipal Natural Science Foundation of Tianjin (13JCYBJC16900, 13JCQNJC08200).

References

1. S. Navalon, M. Alvaro and H. Garcia, *Appl. Catal. B.*, 2010, 99, 1-26.

2. C. Zheng, X. Cheng, P. Chen, C. Yang, S. Bao, J. Xia, M. Guo and X. Sun, *Rsc Advances*, 2015, 5, 40872-40883.

3. M. Hartmann, S. Kullmann and H. Keller, *J. Mater. Chem.*, 2010, 20, 9002-9017.

4. A. Dhakshinamoorthy, S. Navalon, M. Alvaro and H. Garcia, *ChemSusChem*, 2012, 5, 46-64.

5. M. C. Pereira, L. C. A. Oliveira and E. Murad, *Clay Miner.*, 2012, 47, 285-302.

6. S. Rahim Pouran, A. A. Abdul Raman and W. M. A. Wan Daud, *J. Clean. Prod.*, 2014, 64, 24-35.

7. E. G. Garrido-Ramirez, B. K. G. Theng and M. L. Mora, *Appl. Clay Sci.*, 2010, 47, 182-192.

8. S. Navalon, A. Dhakshinamoorthy, M. Alvaro and H. Garcia, *ChemSusChem*, 2011, 4, 1712-1730.

9. P. V. Nidheesh, R. Gandhimathi and S. T. Ramesh, *Environ. Sci. Pollut. Res.,* 2013, 20, 2099-2132.

10. J. H. Ramirez, F. J. Maldonado-Hodar, A. F. Perez-Cadenas, C. Moreno-Castilla, C. A. Costa and L. M. Madeira, *Appl. Catal. B.*, 2007, 75, 312-323.

11. C. S. Castro, M. C. Guerreiro, L. C. A. Oliveira, M. Goncalves, A. S. Anastacio and M. Nazzarro, *Appl. Catal. A.*, 2009, 367, 53-58.

12. Y. Wang, H. Zhao, M. Li, J. Fan, G. Zhao, *Appl. Catal. B.*, 2014, 147, 534-545.

13. F. Duarte, F. J. Maldonado-Hodar and L. M. Madeira, *Ind. Eng. Chem. Res.*, 2012,

51, 9218-9226.

14. F. Duarte, F. J. Maldonado-Hodar and L. M. Madeira, *Appl. Catal. B.*, 2013, 129, 264-272.

15. H. Cui, L. Du, P. Guo, B. Zhu and J. Luong, *J. Power Sources*, 2015, 283, 46-53.

16. F. Duarte, V. Morais, F. J. Maldonado-Hodar and L. M. Madeira, *Chem. Eng. J.,* 2013, 232, 34-41.

17. Y. Wang, G. Zhao, S. Chai, H. Zhao and Y. Wang, *Acs Appl. Mater. Inter.*, 2013, 5, 6773-6773.

18. F. Schuth, *Chem. Mat.*, 2001, 13, 3184-3195.

19. Y. Deng, Y. Cai, Z. Sun, D. Gu, J. Wei, W. Li, X. Guo, J. Yang and D. Zhao, *Adv. Funct. Mater.*, 2010, 20, 3658-3665.

20. C. Liang, Z. Li, and S. Dai, *Angew. Chem. Int. Ed.*, 2008, 47, 3696-3717.

21. B. C. Kim, J. Lee, W. Um, J. Kim, J. Joo, J. H. Lee, J. H. Kwak, J. H. Kim, C. Lee, H. Lee, R. S. Addleman, T. Hyeon, M. B. Gu and J. Kim, *J. Hazard. Mater.*, 2011, 192, 1140-1147.

22. Y. Lin and C. Chang, *Rsc Advances*, 2014, 4, 28628-28631.

23. Y. Wang, H. Zhao and G. Zhao, *Appl. Catal. B.*, 2015, 164, 396-406.

24. Y. Zhai, Y. Dou, X. Liu, B. Tu, and D. Zhao, *J. Mater. Chem.*, 2009, 19, 3292-3300.

25. Y. Meng, D. Gu, F. Q. Zhang, Y. Shi, H. Yang, Z. Li, C. Yu, B. Tu and D. Zhao, *Angew. Chem. Int. Ed.*, 2005, 44, 7053-7059.

26. Z. Sun, B. Sun, M. Qiao, J. Wei, Q. Yue, C. Wang, Y. Deng, S. Kaliaguine and D.

Zhao, *J. Amer. Chem. Soc.*, 2012, 134, 17653-17660.

27. K. Ishibashi, A. Fujishima, T. Watanabe and K. Hashimoto, *J. Photochem. Photobil. A*, 2000, 134, 139-142.

28. R. Moreno-Tovar, E. Terres and J. Rene Rangel-Mendez, *Appl. Surf. Sci.*, 2014, 303, 373-380.

29. P. V. Nidheesh, R. Gandhimathi, S. Velmathi and N. S. Sanjini, *Rsc Advances*, 2014, 4, 5698-5708.

30. P. V. Nidheesh, *Rsc Advances*, 2015, 5, 40552-40577.

31. S. Hanumansetty, E. O'Rear and D. E. Resasco, *Colloids Surf. A*, 2015, 474, 1-8.

32. J. Gao, S. Gao, C. Liu, Z. Liu and W. Dong, *Mater. Res. Bull.*, 2014, 59, 131-136.

33. P. A. Bazula, A. Lu, J. Nitz and F. Schueth, *Microporous Mesoporous Mater.*, 2008, 108, 266-275.

34. A. Sanchez-Sanchez, F. Suarez-Garcia, A. Martinez-Alonso and J. M. D. Tascon, *Appl. Surf. Sci.*, 2014, 299, 19-28.

35. Y. Wang, H. Zhao, M. Li, J. Fan and G. Zhao, *Appl. Catal. B.*, 2014, 147, 534-545.

36. L. Xu and J. Wang, *Appl. Catal. B.*, 2012, 123, 117-126.

37. J. Zhang, H. Zou, Q. Qing, Y. Yang, Q. Li, Z. Liu, X. Guo and Z. Du, *J. Phys. Chem. B.*, 2003, 107, 3712-3718.

38. K. Y. A. Lin and F. K. Hsu, *Rsc Advances*, 2015, 5, 50790-50800.

39. Y. Lin, H. Lin, D. Chen, H. Liu, H. Teng and C. Tang, *Mater. Chem. Phys.*, 2005, 90, 339-343.

40. A. Rodriguez, G. Ovejero, J. L. Sotelo, M. Mestanza, J. Garcia, *Ind. Eng. Chem.*

Res., 2010, 49, 498-505.

41. J. V. Coelho, M. S. Guedes, R. G. Prado, J. Tronto, J. D. Ardisson, M. C. Pereira and L. C. A. Oliyeira, *Appl. Catal. B.*, 2014, 144, 792-799.

42. V. K. Gupta, I. Ali, T. A. Saleh, A. Nayak and S. Agarwal, *Rsc Advances*, 2012, 2, 6380-6388.

43. M. Zhang, Q. Yao, W. Guan, C. Lu and J. Lin, *J. Phys. Chem. C*, 2014, 118, 10441-10447.

44. P. Shukla, S. Wang, H. Sun, H. Ang and M. Tade, *Chem. Eng. J.*, 2010, 164, 255-260.

45. N. Thi Dung, P. Ngoc Hoa, D. Manh Huy and N. Kim Tham, *J. Hazard. Mater.*, 2011, 185, 653-661.

46 G. Q. Zhang, Y. F. Zhou, Y. L. Yang, *J. Electrochem. Soc.*, 2015, 162, H357-H365.

47. L. Gu, N. Zhu, H. Guo, S. Huang, Z. Lou and H. Yuan, *J. Hazard. Mater.*, 2013, 246, 145-153.

48. F. Duarte, F. J. Maldonado-Hodar, A. F. Perez-Cadenas and L. M. Madeira, *Appl. Catal. B*, 2009, 85, 139-147.

49. L. Liu, G. Zhang, L. Wang, T. Huang and L. Qin, *Ind. Eng. Chem. Res.*, 2011, 50, 7219-7227.

50. L. Zhou, J. Ma, H. Zhang, Y. Shao and Y. Li, *Appl. Surf. Sci.*, 2015, 324, 490-498.

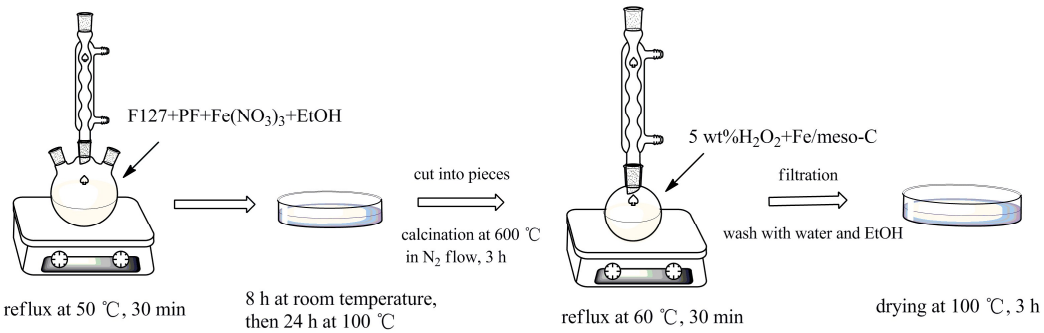

Fig. 1. Schematic illustration of the fabrication of ordered mesoporous carbon catalyst containing uniform iron oxide nanoparticles (Fe/meso-C) and modification by 5 wt% H_2O_2 solution (H-Fe/meso-C).

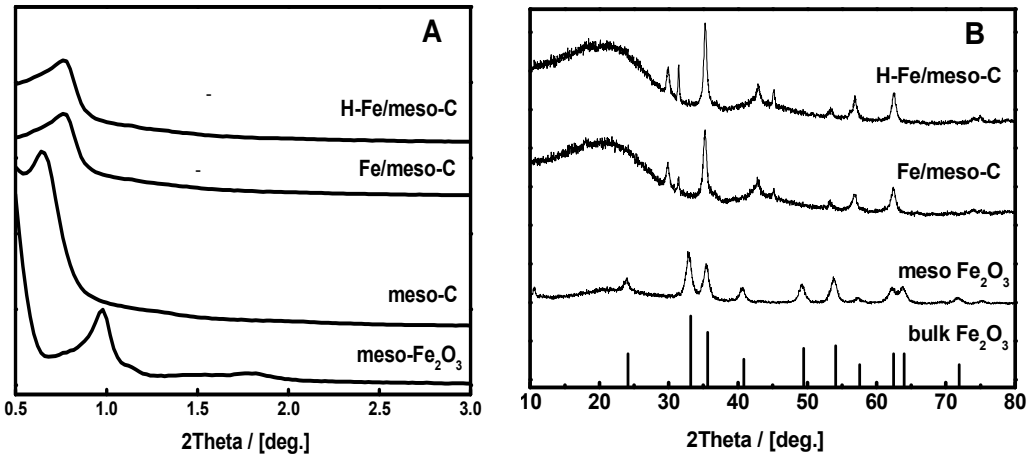

Fig. 2. Small angle XRD patterns (A) of meso-Fe_2O_3, meso-C, Fe/meso-C and H-Fe/meso-C; wide angle XRD patterns (B) of bulk Fe_2O_3, meso-Fe_2O_3, Fe/meso-C and H-Fe/meso-C.

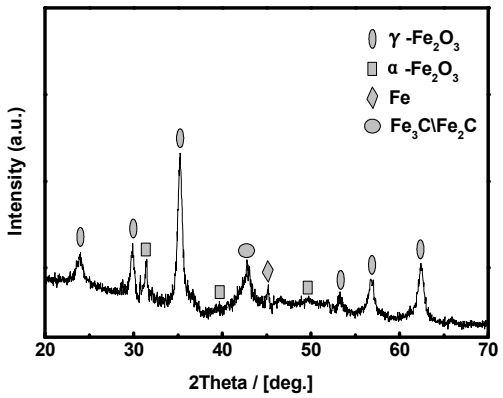

Fig. 3. The wide angle XRD patterns of the H-Fe/meso-C nanoparticles composites carbonized at 800 ºC in N_2.

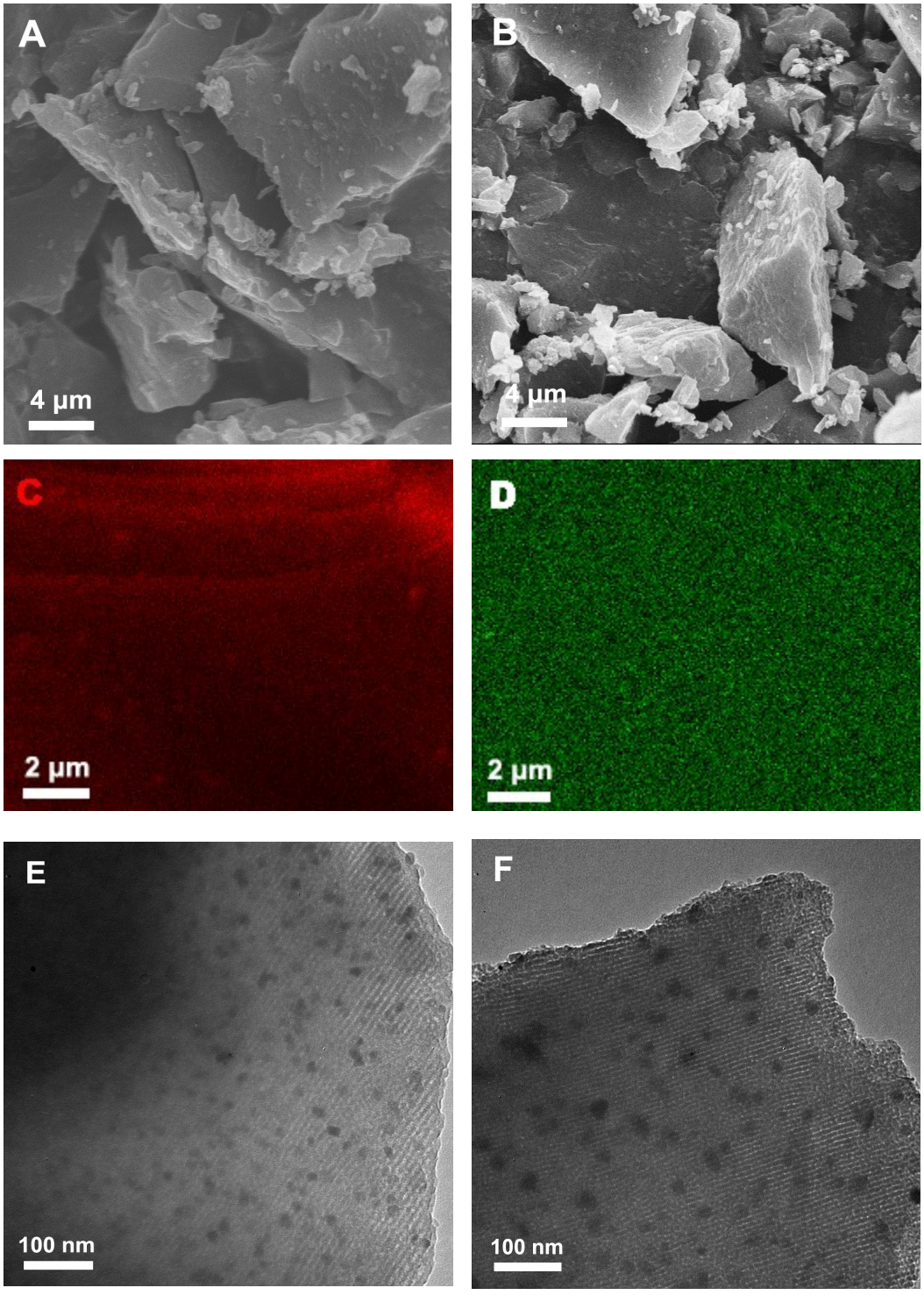

Fig. 4. SEM images of Fe/meso-C (A), H-Fe/meso-C (B); EDS images of C (C) and Fe (D) of H-Fe/meso-C; TEM images of Fe/meso-C (E) and H-Fe/meso-C (F).

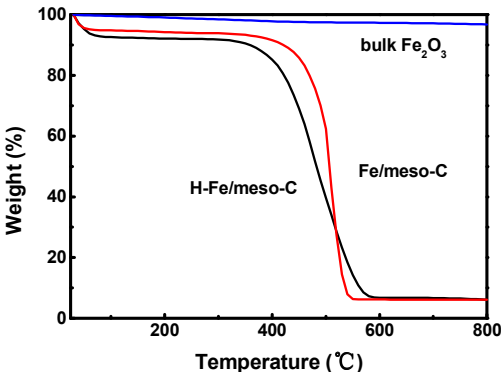

Fig. 5. Thermogravimetric (TG) analysis curves recorded in air for the bulk Fe_2O_3, Fe/meso-C and H-Fe/meso-C.

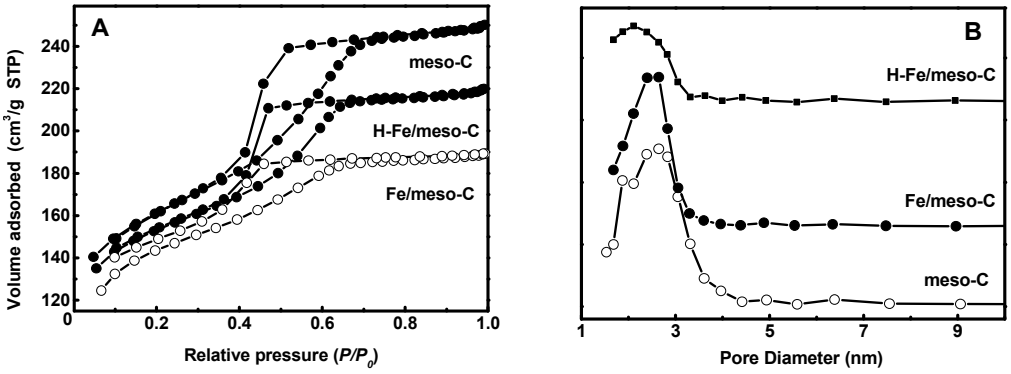

Fig. 6. N_2 adsorption-desorption isotherms at -195 °C (A) and the corresponding pore size distributions (B) of the meso-Fe_2O_3, meso-C, Fe/meso-C and H-Fe/meso-C.

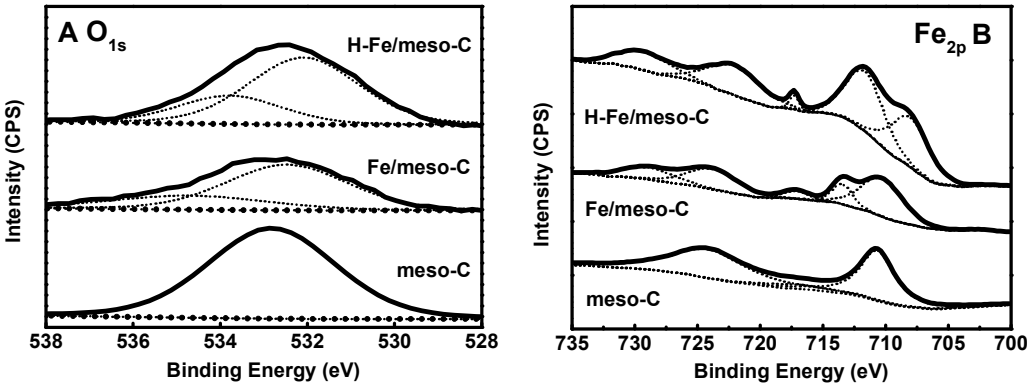

Fig. 7. XPS spectra for O_{1s} regions (A) and Fe_{2p} regions (B) of meso-C, Fe/meso-C and H-Fe/meso-C.

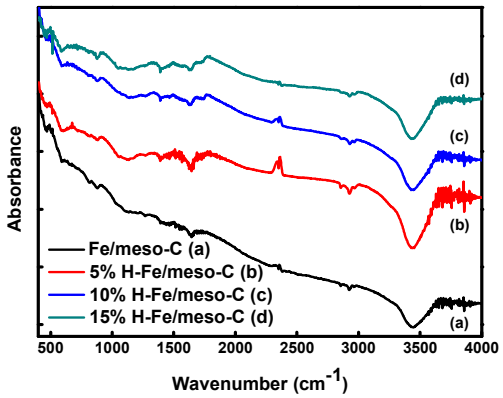

Fig. 8. The FT-IR spectra of Fe/meso-C (a), 5 % H-Fe/meso-C (b), 10 % H-Fe/meso-C (c) and 15 % H-Fe/meso-C (d).

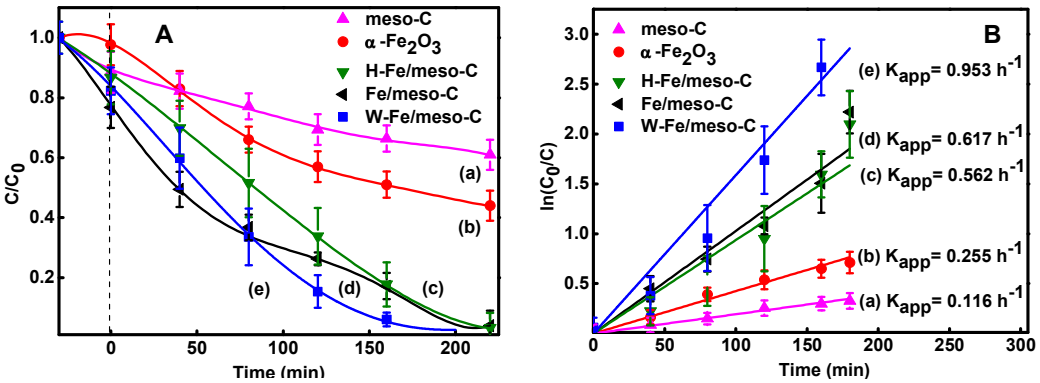

Fig. 9. The degradation efficiency of methylene blue with different catalyst during the reaction (A) and the kinetic curves of methylene blue degradation on the dependence of In(C/C_0) versus time (B). (Except for the investigated parameter, other parameters fixed on initial pH, H_2O_2 concentration 50 mmol, catalyst loading 0.7 g/L, methylene blue concentration 30 mg/L and 25 ℃)

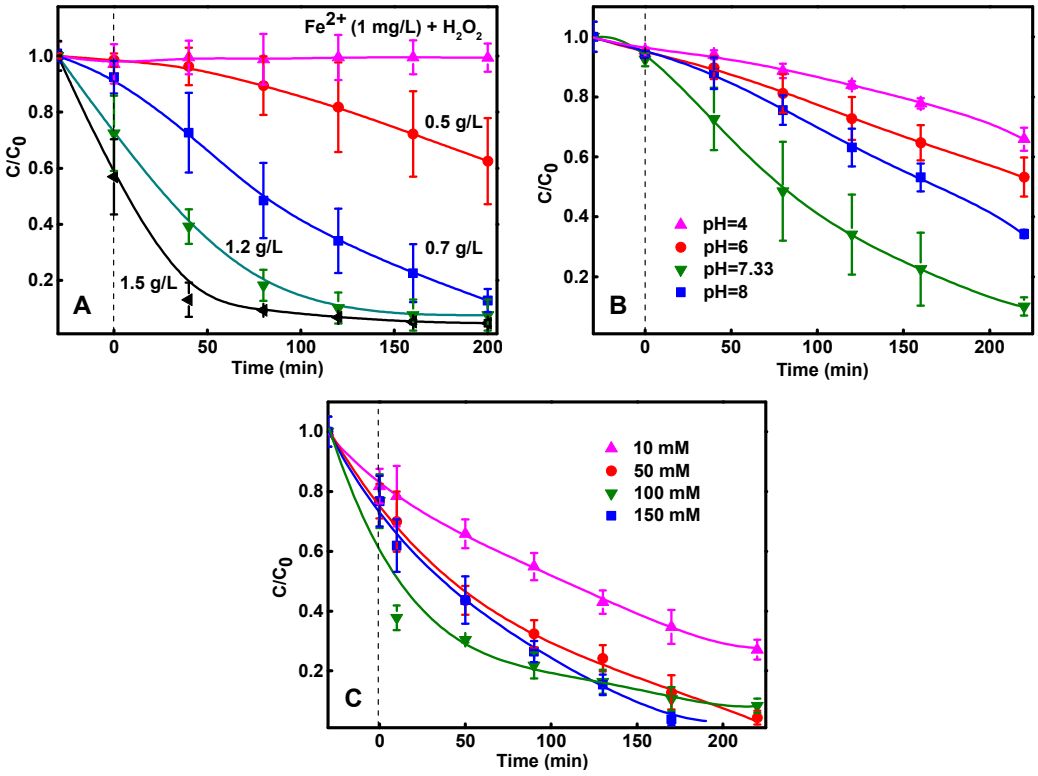

Fig. 10. The degradation of methylene blue in the heterogeneous Fenton processes catalyzed by H-Fe/meso-C: different catalyst loading (A); pH value (B); H_2O_2 initial concentration (C). (Except for the investigated parameter, other parameters fixed on initial pH, H_2O_2 concentration 50 mmol, catalyst loading 0.7 g/L, methylene blue concentration 30 mg/L and 25 °C)

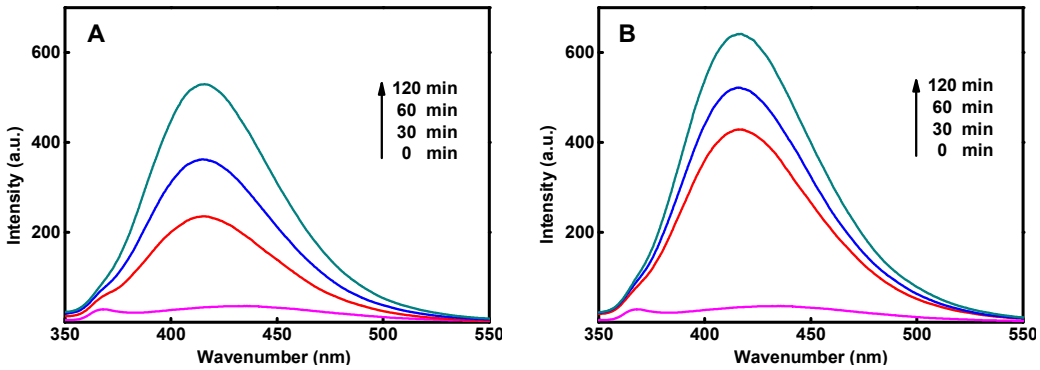

Fig. 11. Total concentrations of ·OH formed as a function of time of Fe/meso-C (A) and H-Fe/meso-C (B). (Except for the investigated parameter, other parameters fixed on initial pH, H_2O_2 concentration 50 mmol, catalyst loading 0.7 g/L, benzoic acid used as a probe at 10 mmol and 25 °C)

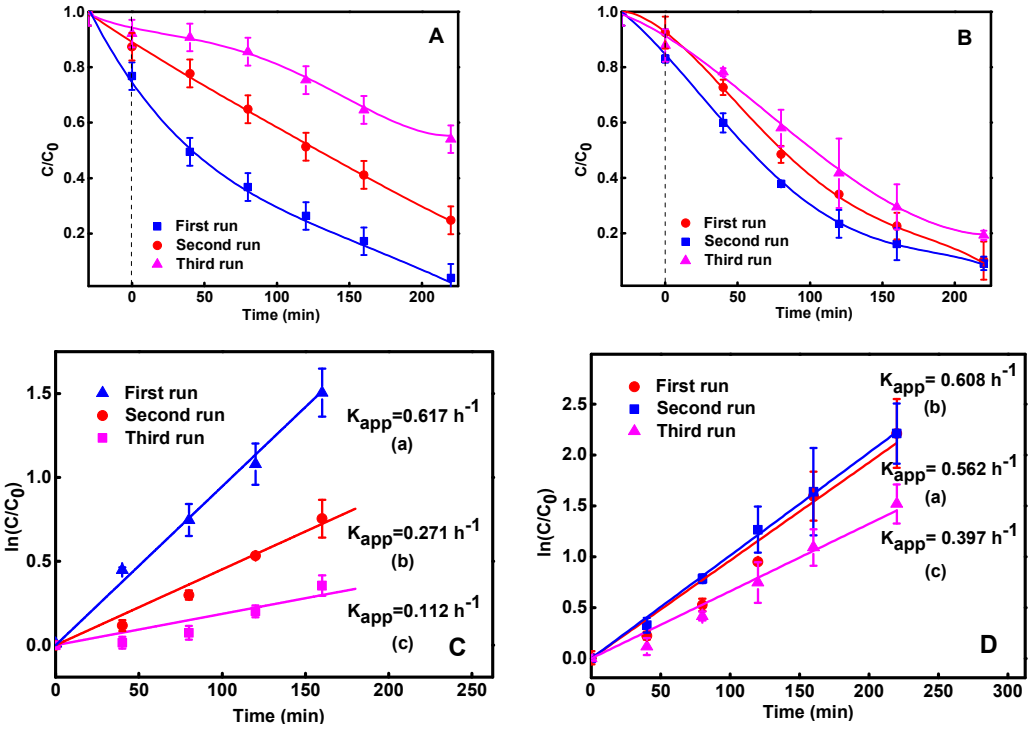

Fig. 12. Degradation of methylene blue with reuse performance of Fe/meso-C (A) and H-Fe/meso-C (B); the kinetic curves of methylene blue degradation on the dependence of ln(C/C_0) versus time of Fe/meso-C (C) and H-Fe/meso-C (D). (Except for the investigated parameter, other parameters fixed on initial pH, H_2O_2 concentration 50 mmol, catalyst loading 0.7 g/L, methylene blue concentration 30 mg/L and 25 °C)

Table 1. The EDX comparison of the Fe nanoparticles incorporated ordered mesoporous carbon and selected iron-based catalysts

Element	Meso-C	bulk-Fe_2O_3	Fe/meso-C	H-Fe/meso-C
C	92.73%	-	86.31%	83.00%
O	6.81%	14.12%	5.94%	10.7%
Fe	0.46%	85.88%	7.75%	6.3%

Table 2. Structural and textural properties of the Fe nanoparticles incorporated ordered mesoporous carbon and selected iron-based catalysts

Catalyst	S_{BET} ($m^2 \cdot g^{-1}$)	V_{pore} ($cm^3 \cdot g^{-1}$)	V_{micro} ($cm^3 \cdot g^{-1}$)	D_p (nm)	a_0 (nm)	h (nm)	*Contact angle*
Meso-C	516	0.31	0.14	2.1	25.02	22.72	-
Fe/meso-C	532	0.29	0.14	2.1	20.53	18.43	113.49±0.18
5 %H-Fe/meso-C	561	0.29	0.13	2.3	21.07	18.97	116.45±2.66
10 %H-Fe/meso-C	589	0.30	0.13	2.3	-	-	108.05±6.63
15 %H-Fe/meso-C	613	0.31	0.12	2.4	-	-	96.47±5.53